Electronic Supplementary Material (ESI) for Journal of Materials Chemistry C.

Supplementary Materials for
Stable freestanding two-dimensional anionic electrons in YCl with extremely weak interlayer interaction

Zhenghui Fang,[a] Xuguang Wang,[a] Xinyu Cao,[a] Hao Yang,[a] Feifei Yin,[a]

Kai Liu[b] and Xiao Zhang[a]*

[a]State Key Laboratory of Information Photonics and Optical Communications & School of Science, Beijing University of Posts and Telecommunications, Beijing 100876, China

[b]Department of Physics and Beijing Key Laboratory of Opto-electronic Functional Materials & Micro-nano Devices, Renmin University of China, Beijing 100872, China

*Corresponding author: zhangxiaobupt@bupt.edu.cn

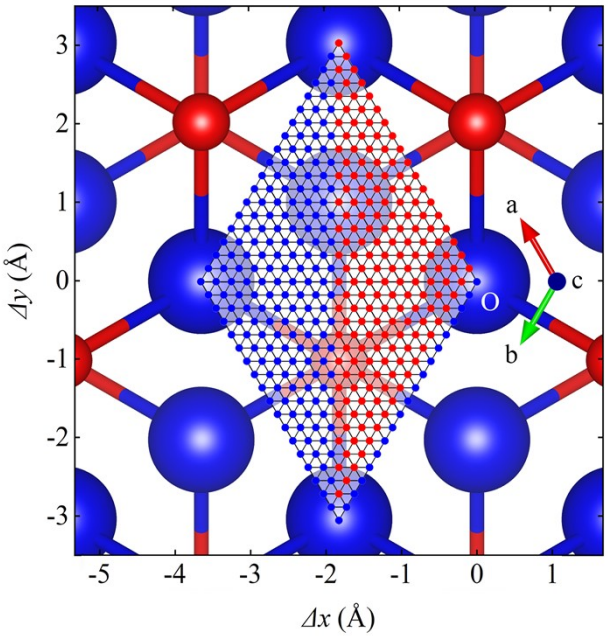

Figure S1. Schematic diagram of each sampled structure in the simulation of the quasi-static process of relative sliding between YCl bilayers. When stacked in AA sequence, the relative sliding between the layers of the YCl bilayer is considered as zero, corresponding to the origin of the coordinates (marked as O). One sampling structure is taken for every $a/18$ (0.20 Å) sliding of the upper layer with respect to the fixed lower layer (ML YCl in the background), corresponding to the intersection point in the rhombic grid. The displacement of the relative sliding between the layers of each sampling structure is the distance from its corresponding intersection point to the origin. Considering symmetry, all points corresponding to irreducible structures are marked in red.

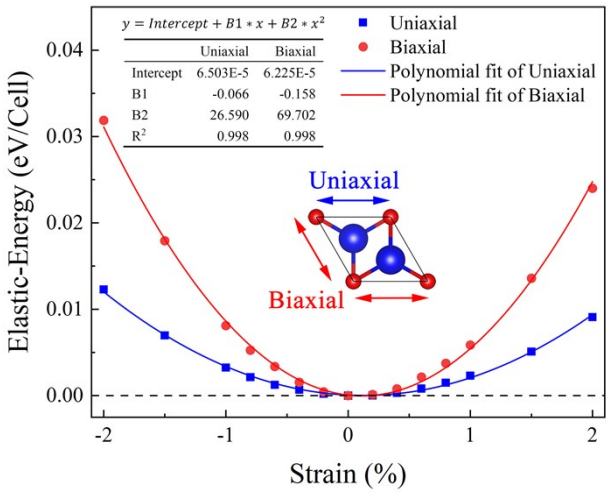

Figure S2. The elastic energy curves of ML YCl under applied uniaxial and biaxial strains and their second-order polynomial fitting curves. Insets: parameters of the second-order polynomial fit and schematic diagrams of applied uniaxial and biaxial strains.

The in-plane second-order elastic constants play a crucial role in understanding the mechanical and dynamic properties of 2D materials by providing information on material stiffness and stability. Applying a small strain to the equilibrium lattice configuration in the linear elastic region, the elastic energy change of a 2D material in the harmonic approximation can be given by the following formula [1]

$$E_{elastic}^{2D} = S\left(\frac{1}{2}C_{11}\varepsilon_1^2 + \frac{1}{2}C_{22}\varepsilon_2^2 + C_{12}\varepsilon_1\varepsilon_2 + 2C_{16}\varepsilon_1\varepsilon_6 + 2C_{26}\varepsilon_2\varepsilon_6 + 2C_{66}\varepsilon_6^2\right)$$

where $E_{elastic}^{2D}$ is the difference between the total energy of the equilibrium and distorted lattice cells, S is the area of the equilibrium 2D material, $C_{ij}\ (i,j\ = 1,2,6)$ is the in-plane stiffness tensor in N/m, and $\varepsilon_i\ (i\ = 1,2,6)$ is the independent component of the strain tensor $\boldsymbol{\varepsilon}$. The lattice vector relationship between the distorted lattice and the equilibrium lattice is given by

$$\begin{pmatrix} a' \\ b' \\ c' \end{pmatrix} = \begin{pmatrix} a \\ b \\ c \end{pmatrix} \cdot (I + \varepsilon)$$

where $\boldsymbol{I}$ is the unit matrix. The strain tensor $\boldsymbol{\varepsilon}$ is expressed as the following vector with six independent components

$$\varepsilon = \begin{pmatrix} \varepsilon_1 & \frac{\varepsilon_6}{2} & \frac{\varepsilon_5}{2} \\ \frac{\varepsilon_6}{2} & \varepsilon_2 & \frac{\varepsilon_4}{2} \\ \frac{\varepsilon_5}{2} & \frac{\varepsilon_4}{2} & \varepsilon_3 \end{pmatrix}$$

As a 2D material, the ML YCl belongs to the hexagonal crystal system, which has only two independent elastic constants C_{11} and C_{12} considering symmetry.[2] In the energy-strain approach, the elastic constants can be derived from the quadratic coefficients of the elastic energy-strain curve. To obtain the elastic constant C_{11}, a uniaxial strain along the a-axis is applied to the equilibrium

lattice

$$\varepsilon_{Uniaxial} = \begin{pmatrix} \varepsilon_1 & 0 & 0 \\ 0 & 0 & 0 \\ 0 & 0 & 0 \end{pmatrix}$$

The elastic energy of the ML YCl under uniaxial strain is

$$E_{Uniaxial}^{2D} = S(\frac{1}{2}C_{11}\varepsilon_1^2)$$

Comparing the quadratic coefficients of the elastic energy-uniaxial strain fitting curve (i.e., the blue curve in Fig. S2), C_{11} = 74.289 N/m can be obtained. Similarly, to obtain the constant C_{12}, an equal biaxial strain along the *a* and *b* axes is applied to the equilibrium lattice

$$\varepsilon_{Biaxial} = \begin{pmatrix} \varepsilon_1 & 0 & 0 \\ 0 & \varepsilon_2 & 0 \\ 0 & 0 & 0 \end{pmatrix} = \begin{pmatrix} \varepsilon_1 & 0 & 0 \\ 0 & \varepsilon_1 & 0 \\ 0 & 0 & 0 \end{pmatrix}$$

The elastic energy of the ML YCl under biaxial strain is

$$E_{Biaxial}^{2D} = S\left(\frac{1}{2}C_{11}\varepsilon_1^2 + \frac{1}{2}C_{22}\varepsilon_2^2 + C_{12}\varepsilon_1\varepsilon_2\right) = S\left(C_{11}\varepsilon_1^2 + C_{12}\varepsilon_1\varepsilon_2\right) = S(C_{11} + C_{12})\varepsilon_1^2$$

Comparing the quadratic coefficients of the elastic energy-biaxial strain fitting curve (i.e., the red curve in Fig. S2) and C_{11}, C_{12} = 23.076 N/m can be obtained. The two calculated elastic constants satisfy the mechanical stability criterion: $C_{11} > 0$ and $C_{11} > |C_{12}|$, meaning that the ML YCl is mechanically stable.[2] Using these known elastic constants, the in-plane Young's modulus (Y_{2D}), shear modulus (G_{2D}), and Poisson's ratio (v_{2D}) of YCl can be obtained as follows

$$\begin{cases} Y_{2D} = \dfrac{C_{11}^2 - C_{12}^2}{C_{11}} = 67.121\ N/m \\ G_{2D} = \dfrac{C_{11} - C_{12}}{2} = 25.606\ N/m \\ v_{2D} = \dfrac{C_{12}}{C_{11}} = 0.311 \end{cases}$$

The vertical deformation *h* occurring under gravity in an independent ML YCl of size *l* can be estimated by the following equation [1]

$$\frac{h}{l} \approx \left(\frac{\rho g l}{Y_{2D}}\right)^{\frac{1}{3}}$$

where *g* is the gravitational acceleration, ρ is the density of ML YCl (ρ = 1.29 × 10^{-4} kg m^{-2}). It is found that the ratio of vertical deformation to film size *h*/*l* is only 1.23 × 10^{-3} even for a large YCl film with *l* = 100 μm. This result indicates that the in-plane stiffness of ML YCl is sufficient to avoid curling and makes itself form a freestanding film.

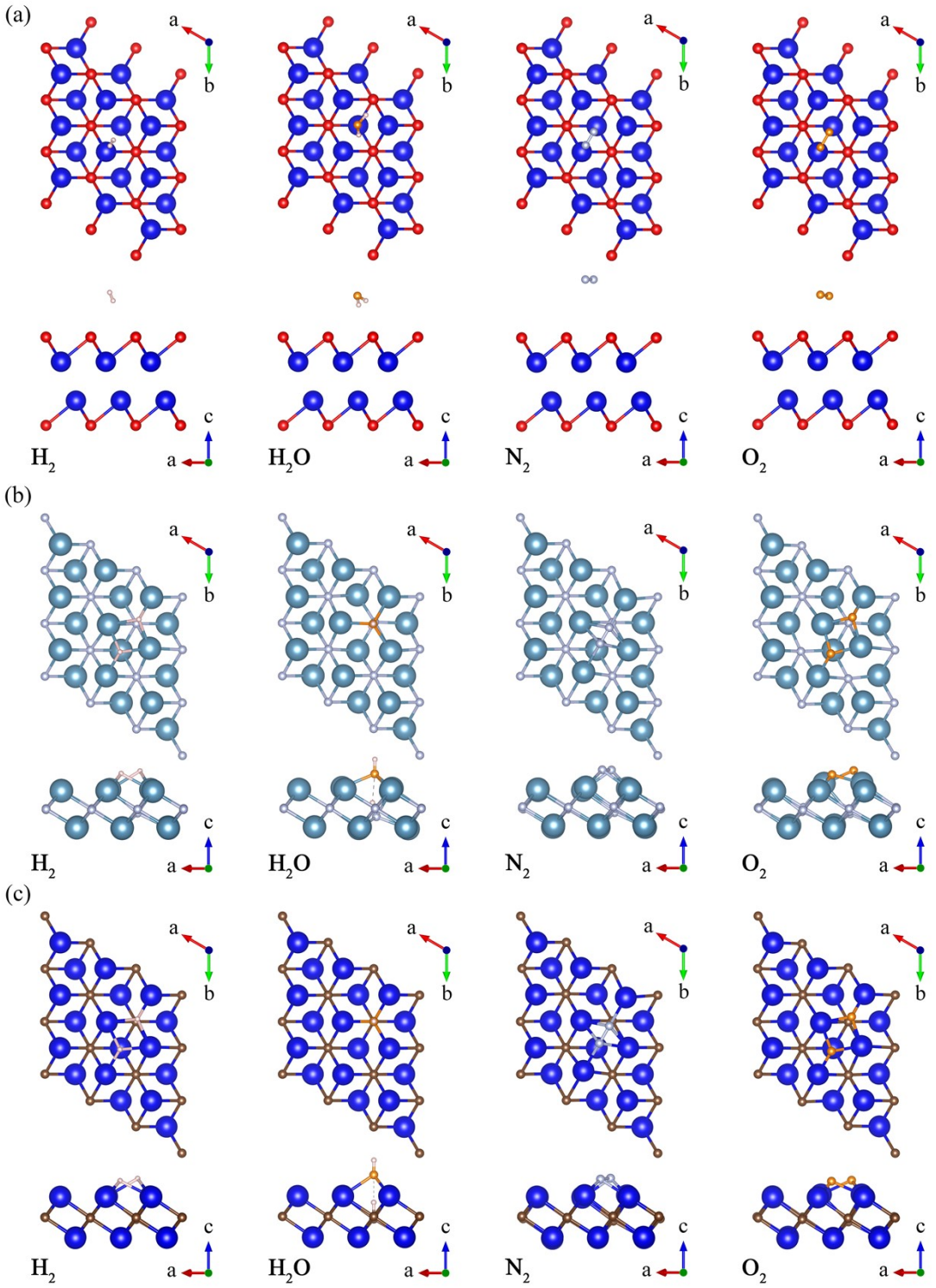

Figure S3. Top and side views of H_2, H_2O, N_2, and O_2 absorbed on the ML (a) YCl, (b) Ca_2N, and (c) Y_2C. Red, blue, cyan, brown, white, orange, and silver balls denote chlorine, yttrium, calcium, carbon, hydrogen, oxygen, and nitrogen atoms, respectively.

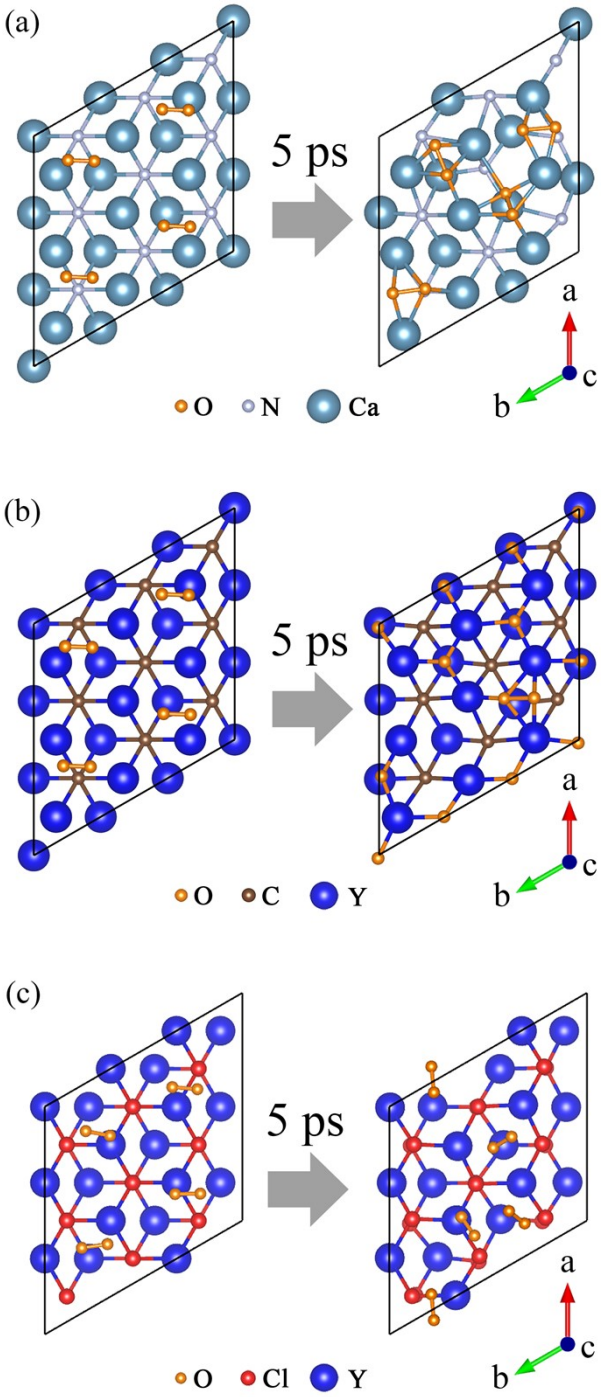

Figure S4. Top views of the initial and final snapshots of 2D systems with gaseous phase oxygen after 5.0 ps AIMD simulations at the temperature of 300 K for ML (a) Ca_2N, (b) Y_2C, and (c) YCl.

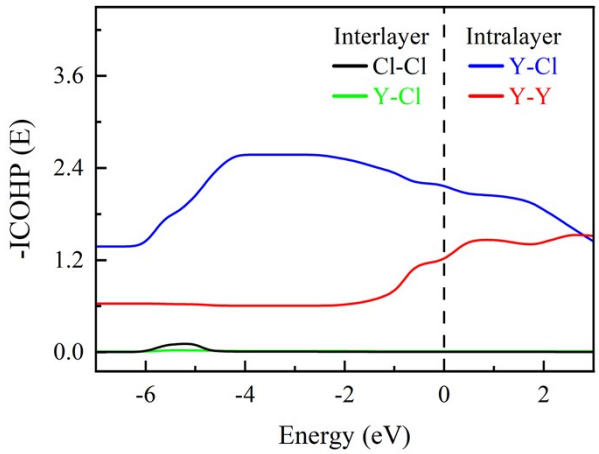

Figure S5. The integral of the COHP (ICOHP) of the local chemical bonds between the atoms in the bulk YCl.

Table S1. Easily exfoliated binaries with up to six atoms per unit cell.[3] If a 2D substructure can be exfoliated from multiple 3D parents, the most easily exfoliated ones (corresponding to the smallest E_b) are listed. In this table, binaries that do not have sandwich-like structures wrapped by chalcogen and halogen elements are marked with the asterisk.

	Formula	Space group	E_b (meV/Å^2)		Experimental 3D parent structure(s)		
			DF2-C09	rVV10	Formula	Source DB	DB ID
*	SiH	$P\bar{3}m1$	9.0	13.0	Si_2H_2	ICSD	41478
*	BN	$P\bar{6}m2$	19.4	24.4	B_2N_2	ICSD	186248
*	W_2N_3	$P\bar{6}m2$	26.3	39.8	W_4N_6	ICSD	186207
*	PbO	$P4/nmm$	7.8	14.3	$Ag_2Pb_2O_2Br_2$	ICSD	33913
	FeO_2	$Pmmn$	16.3	29.8	Fe_2O_4	COD	9015156
	NiO_2	$P\bar{3}m1$	16.6	27.6	NiO_2	COD	1522025
	PtO_2	$P\bar{3}m1$	19.3	32.3	Pt_2O_4	ICSD	24923
	Tl_2O	$P\bar{3}m1$	19.4	27.3	Tl_4O_2	COD	1528007
	CoO_2	$P\bar{3}m1$	22.6	34.3	CoO_2	COD	1522027
*	SnO	$P4/nmm$	29.8	34.6	Sn_2O_2	COD	7206470
	SnO	$C2/m$	-	28.4	Sn_4O_4	ICSD	424729
	GaS	$P\bar{6}m2$	15.8	20.8	Ga_4S_4	ICSD	635254
	GaS	$P\bar{3}m1$	16.1	20.8	Ga_2S_2	ICSD	40824
	SnS_2	$P\bar{3}m1$	16.7	23.7	Sn_2S_4	ICSD	43003
	HfS_2	$P\bar{3}m1$	18.2	23.2	HfS_2	ICSD	638847
	ZrS_2	$P\bar{3}m1$	19.0	24.1	ZrS_2	COD	5910006
	Tl_2S	$P\bar{3}m1$	19.2	-	Tl_2S	COD	9012278
	MoS_2	$P\bar{6}m2$	21.6	28.8	Mo_2S_4	ICSD	644259
	TaS_2	$P\bar{3}m1$	22.3	27.6	TaS_2	COD	9011539
	WS_2	$P\bar{6}m2$	22.7	29.9	WS_2	COD	9012192
	NbS_2	$P\bar{3}m1$	23.2	28.0	NbS_2	ICSD	24755
	TaS_2	$P\bar{6}m2$	23.2	28.6	TaS_2	ICSD	651083
	FeS	$P4/nmm$	23.3	29.4	Fe_2S_2	COD	9011800
	TiS_2	$P\bar{3}m1$	23.8	27.4	TiS_2	COD	1010275
	NbS_2	$P\bar{6}m2$	24.3	29.0	NbS_2	ICSD	237034
*	PdS_2	$P2_1/c$	27.1	31.5	Pd_4S_8	COD	2310589
	PtS_2	$P\bar{3}m1$	27.3	33.0	PtS_2	COD	5910085
	VS_2	$P\bar{3}m1$	27.7	31.2	VS_2	ICSD	651361
	MoS_2	$P\bar{3}m1$	28.7	33.5	MoS_2	ICSD	26622
*	GeS	$Pmn2_1$	37.3	34.8	Ge_4S_4	COD	9008784
	InSe	$P\bar{6}m2$	14.9	20.8	In_4Se_4	COD	9008967
	GaSe	$P\bar{6}m2$	15.1	20.4	Ga_4Se_4	COD	9008968
	In_2Se_3	$C2$	16.1	23.5	In_2Se_3	ICSD	602266
	$SnSe_2$	$P\bar{3}m1$	17.3	25.0	$SnSe_2$	ICSD	43857
	$HfSe_2$	$P\bar{3}m1$	18.8	23.9	$HfSe_2$	ICSD	182678
	Bi_2Se_3	$P\bar{3}m1$	19.6	26.6	Bi_2Se_3	COD	9011965
	$ZrSe_2$	$P\bar{3}m1$	20.0	25.0	$ZrSe_2$	COD	5910026
	$MoSe_2$	$P\bar{6}m2$	20.4	28.4	Mo_2Se_4	ICSD	644346

	$TaSe_2$	$P\bar{6}m2$	22.6	28.2	Ta_2Se_4	ICSD	651956
	WSe_2	$P\bar{6}m2$	22.6	30.0	W_2Se_4	COD	9012193
	FeSe	$P4/nmm$	22.6	29.3	Fe_2Se_2	ICSD	290411
	$TaSe_2$	$P\bar{3}m1$	23.1	29.1	$TaSe_2$	ICSD	651954
	$CrSe_2$	$C2/m$	23.3	29.7	$CrSe_2$	ICSD	626718
	$NbSe_2$	$P\bar{6}m2$	23.5	28.8	Nb_2Se_4	COD	9014575
	$TiSe_2$	$P\bar{3}m1$	24.0	28.2	$TiSe_2$	COD	1010276
	VSe_2	$P\bar{3}m1$	25.4	30.2	VSe_2	ICSD	86520
	$NbSe_2$	$P\bar{3}m1$	27.1	32.0	$NbSe_2$	ICSD	76576
	AuSe	$P2/m$	27.7	33.3	Au_2Se_2	COD	1510294
	$ReSe_2$	$P\bar{6}m2$	28.3	30.3	Re_4Se_8	ICSD	650091
	$PtSe_2$	$P\bar{3}m1$	29.6	35.2	$PtSe_2$	COD	9009117
	InSe	$C2/m$	32.7	33.7	In_2Se_2	ICSD	32714
*	GeSe	$Pmn2_1$	36.0	33.9	Ge_4Se_4	COD	1528768
	Cu_2Te	$C2/m$	14.6	20.5	Cu_4Te_2	ICSD	77055
	GaTe	$P\bar{6}m2$	15.7	20.6	Ga_4Te_4	ICSD	43328
	$SiTe_2$	$P\bar{3}m1$	19.9	25.6	$SiTe_2$	COD	9009119
	WTe_2	$P2_1/m$	22.1	28.4	W_4Te_8	COD	2310355
	CuTe	$Pmmn$	22.2	27.0	Cu_2Te_2	COD	1526237
	Bi_2Te_3	$P\bar{3}m1$	23.0	28.7	$SnBi_4Te_7$	ICSD	236253
	$HfTe_2$	$P\bar{3}m1$	23.4	26.4	$HfTe_2$	ICSD	603713
	$MoTe_2$	$P2_1/m$	24.5	30.1	Mo_4Te_8	COD	2310356
	WTe_2	$P\bar{6}m2$	24.7	30.0	W_2Te_4	ICSD	653170
	$MoTe_2$	$P\bar{6}m2$	25.2	30.4	Mo_2Te_4	COD	9009147
	Sb_2Te_3	$P\bar{3}m1$	25.2	30.0	Sb_2Te_3	COD	9007590
	$ZrTe_2$	$P\bar{3}m1$	26.1	28.4	$ZrTe_2$	ICSD	653213
	FeTe	$P4/nmm$	26.6	31.6	Fe_2Te_2	ICSD	169974
	VTe_2	$P\bar{3}m1$	27.1	30.1	VTe_2	ICSD	603582
*	PbTe	$P3m1$	27.5	33.0	$Pb_2Bi_2Te_5$	ICSD	42708
	$TiTe_2$	$P\bar{3}m1$	28.1	30.2	$TiTe_2$	COD	1008063
	$NbTe_2$	$P\bar{3}m1$	28.3	31.8	$NbTe_2$	ICSD	645529
	Hf_3Te_2	$P4/mmm$	31.7	33.1	Hf_3Te_2	ICSD	75936
*	SnTe	$Pmn2_1$	34.2	33.2	Sn_4Te_4	ICSD	652743
*	TlF	$P4/nmm$	14.1	20.1	Tl_2F_2	COD	1520825
	NbF_4	$P4/mmm$	15.1	29.1	NbF_4	ICSD	25768
	PbF_4	$P4/mmm$	15.7	29.0	PbF_4	COD	1528583
	SnF_4	$P4/mmm$	22.8	33.3	SnF_4	COD	1528582
*	AgF_2	$P2_1/c$	28.2	42.5	Ag_4F_8	COD	1509321
	$FeCl_2$	$P\bar{3}m1$	9.7	15.2	$FeCl_2$	COD	9014952
	$ZnCl_2$	$P\bar{4}m2$	9.8	15.9	Zn_2Cl_4	ICSD	26152
	$CoCl_2$	$P\bar{3}m1$	10.7	15.9	$CoCl_2$	COD	9014719
	$CdCl_2$	$P\bar{3}m1$	11.0	17.8	$CdCl_2$	COD	9009125
	LaCl	$P\bar{3}m1$	11.0	16.8	La_2Cl_2	ICSD	24410
	$ZnCl_2$	$P\bar{3}m1$	11.1	16.8	$ZnCl_2$	COD	9009136

	TbCl	$P\bar{3}m1$	11.2	-	Tb_2Cl_2	ICSD	23351
	YCl	$P\bar{3}m1$	12.0	17.6	Y_2Cl_2	ICSD	30708
	$MgCl_2$	$P\bar{3}m1$	12.3	17.7	$MgCl_2$	COD	9009129
	$CuCl_2$	$C2/m$	13.4	19.7	$CuCl_2$	COD	9001506
	ScCl	$P\bar{3}m1$	13.8	19.4	Sc_2Cl_2	COD	4343683
	$PdCl_2$	$P2_1/c$	14.0	21.3	Pd_2Cl_4	ICSD	421221
	RbCl	$P4/nmm$	14.4	18.7	$Rb_2Ni_2C_4N_4Cl_2$	ICSD	380471
	$ZrCl_2$	$P\bar{6}m2$	14.5	21.4	$ZrCl_2$	ICSD	30052
	ZrCl	$P\bar{3}m1$	14.7	21.8	Zr_2Cl_2	ICSD	20145
	$MnCl_2$	$C2/m$	14.8	21.5	$MnCl_2$	COD	9009130
	$TiCl_2$	$P\bar{3}m1$	14.9	21.6	$TiCl_2$	COD	9009121
	VCl_2	$C2/m$	15.5	22.1	VCl_2	COD	1528165
	$NiCl_2$	$P\bar{3}m1$	16.3	22.6	$NiCl_2$	COD	9009132
*	AgBr	$P2_1/m$	7.8	14.3	$Ag_2Pb_2O_2Br_2$	ICSD	33913
	$MgBr_2$	$P\bar{3}m1$	10.2	15.3	$MgBr_2$	COD	8103685
	$CdBr_2$	$P\bar{3}m1$	10.8	17.5	$CdBr_2$	COD	9009124
	$LaBr_2$	$P\bar{6}m2$	11.2	16.8	La_2Br_4	ICSD	65481
	$ZnBr_2$	$P\bar{3}m1$	11.4	20.0	$ZnBr_2$	COD	9011540
	LaBr	$P\bar{3}m1$	11.7	17.5	La_2Br_2	ICSD	23354
	TbBr	$P\bar{3}m1$	12.2	17.9	Tb_2Br_2	ICSD	23353
	AuBr	$Cmme$	12.7	21.0	Au_4Br_4	COD	1510610
	$MnBr_2$	$C2/m$	15.0	21.6	$MnBr_2$	ICSD	67500
	$TiBr_2$	$P\bar{3}m1$	15.3	21.8	$TiBr_2$	ICSD	26078
	$FeBr_2$	$P\bar{3}m1$	15.5	22.2	$FeBr_2$	COD	9009102
	CuBr	$P4/nmm$	15.5	22.9	Cu_2Br_2	COD	9013931
	$CrBr_2$	$P\bar{1}$	15.5	22.0	$CrBr_2$	ICSD	23903
	ZrBr	$P\bar{3}m1$	15.6	22.5	Zr_2Br_2	COD	4343762
	VBr_2	$C2/m$	15.8	22.1	VBr_2	ICSD	246906
	$CoBr_2$	$P\bar{3}m1$	16.8	23.3	$CoBr_2$	COD	9016149
	$NiBr_2$	$P\bar{3}m1$	18.1	24.4	$NiBr_2$	COD	9008013
	PbI_2	$P\bar{3}m1$	8.6	16.1	Pb_2I_4	COD	9009143
	GeI_2	$P\bar{6}m2$	8.8	13.3	GeI_2	COD	1010319
	CaI_2	$P\bar{3}m1$	9.9	15.3	CaI_2	COD	9009097
	TmI_2	$P\bar{3}m1$	10.5	16.1	TmI_2	ICSD	43731
	YbI_2	$P\bar{3}m1$	10.6	16.1	YbI_2	ICSD	77907
	CdI_2	$P\bar{3}m1$	10.7	17.2	Cd_3I_6	ICSD	20745
	MgI_2	$P\bar{3}m1$	10.8	16.2	MgI_2	COD	9009108
	HgI_2	$P\bar{4}m2$	11.5	18.8	Hg_2I_4	COD	9014434
	ZnI_2	$P\bar{3}m1$	11.7	17.4	ZnI_2	COD	9009137
	GeI_2	$P\bar{3}m1$	12.1	17.6	Ge_3I_6	ICSD	23176
	AgI	$P4/nmm$	13.5	20.8	Ag_2I_2	COD	1509387
	CuI	$P\bar{3}m1$	14.7	20.9	Cu_6I_6	ICSD	30363
	ZrI_2	$P2_1/m$	14.8	21.0	Zr_4I_8	ICSD	26418
	CuI	$C2/m$	14.8	21.7	Cu_2I_2	COD	9013923

AuI	*Cmme*	15.1	22.4	Au_4I_4	COD	9008986
LaI_2	*P*4/*mmm*	15.6	21.2	LaI_2	COD	1529708
VI_2	*C*2/*m*	16.4	22.4	VI_2	ICSD	246907
NdI_2	*P*4/*mmm*	16.4	21.9	NdI_2	ICSD	72190
CrI_2	$P2_1/m$	16.8	22.5	CrI_2	ICSD	4073
FeI_2	$P\bar{3}m1$	16.9	23.3	FeI_2	COD	9009103
MnI_2	*C*2/*m*	17.0	23.3	MnI_2	COD	9009110
CoI_2	*C*2/*m*	18.3	24.3	CoI_2	COD	9009100
SrI_2	*Pmmm*	21.2	26.6	Sr_4I_8	ICSD	203137
NiI_2	$P\bar{3}m1$	21.5	26.9	NiI_2	COD	9009133

References:

[1] L. D. Landau and E. M. Lifshitz, Course of Theoretical Physics Vol 7: Theory and Elasticity, Elsevier, 2013.

[2] M. Maździarz, Comment on 'The Computational 2D Materials Database: high-throughput modeling and discovery of atomically thin crystals', *2D Mater.*, 2019, **6**(4), 048001.

[3] N. Mounet, M. Gibertini, P. Schwaller, D. Campi, A. Merkys, A. Marrazzo, T. Sohier, I. E. Castelli, A. Cepellotti and G. Pizzi, Two-dimensional materials from high-throughput computational exfoliation of experimentally known compounds, *Nat. Nanotechnol.*, 2018, **13**(3), 246-252.